Numerical and experimental study of circulation flow rate in a closed circuit due to gas jet impingement

P. Anil Kishan and Sukanta K. Dash
Department of Mechanical Engineering, IIT Kharagpur, Kharagpur, India

Abstract

Purpose – The purpose of the present investigation is to compute the circulation flow of a liquid in a closed chamber when the liquid is fired by a gas jet through number of nozzles.

Design/methodology/approach – The conservation equations for mass and momentum have been solved in a closed container along with the conservation of volume fraction of the secondary phase in order to take into account the gas phase present in the liquid. The drag force created by the gas on the liquid has been incorporated in the momentum equation as a source term and the resulting equations have been solved numerically using a finite volume technique in an unstructured grid employing a phase coupled pressure linked velocity solver for the pressure correction equation, which is usually known as the Eulerian Scheme for two phase flow solution. An eddy viscosity based k-ε turbulence model for the mixture was considered to update the fluid viscosity with iterations and capture the turbulence in the overall mixture rather than computing the individual turbulence in both the phases, which was found to be extremely time-consuming and computationally unstable to some extent.

Findings – The model thus developed was tried to predict the circulation flow rate in an experimental setup where air was injected to drive the water in a long U tube setup. The computed circulation flow rate was found to be within 15 percent deviation from the experimentally observed values. The circulation flow rate of water was found to be increasing with the injected airflow rate. After this model validation, circulation flow rate of steel in an industrial size Ruhrstal-Haraeus (RH)-degasser was computed by injecting argon into the liquid steel through the up-leg of the RH vessel. It was found that the circulation flow rate of steel in the RH degasser was increasing when the argon flow was being varied from 800 to 1,600 NL/min, which confirms the industrial findings.

Research limitations/implications – The present computation could not use the energy equation to compute the swelling of the gas bubbles inside the chamber due to huge computing time requirement.

Practical implications – The present computation could compute realistically the circulation flow rate of water in a U tube when fired by a gas jet by using a two-phase Eulerian model and hence this model can be effectively used for industrial applications where two-phase flow comes into picture.

Originality/value – The original contribution of the paper is in the use of the state-of the-art Eulerian two-phase flow model to predict circulation flow in an industrial size RH degasser.

Keywords Modelling, Circulation systems, Experimentation, Gas flow

Paper type Research paper

Nomenclature

C_D = drag coefficient
C_L = lift coefficient
C_{VM} = virtual mass coefficient
d = diameter of bubble
$\vec{g}$ = acceleration due to gravity
G = production of turbulent kinetic energy
k = turbulent kinetic energy

International Journal of Numerical Methods for Heat & Fluid Flow
Vol. 16 No. 8, 2006
pp. 890-909

0961-5539
DOI 10.1108/09615530610702050

M = interfacial forces
M^{d} = drag force
M^{L} = lift force
M^{VM} = virtual mass force
p = pressure
Re = Reynolds number
Γ = mass transfer between phases
α = volume fraction
ρ = density
$\vec{v}$ = velocity vector
$\bar{\bar{\tau}}$ = stress tensor
μ = shear viscosity
μ_t = turbulent viscosity
μ^{eff} = effective viscosity
ε = rate of dissipation
σ_k = turbulent Prandtl number for k
σ_ε = turbulent Prandtl number for ε

Subscripts
q = primary phase (liquid/steel), any phase
p = secondary phase (gas/argon)
m = mixture

Introduction

The Ruhrstal-Haraeus (RH) degasser is one of the various vacuum degassing processes which has gained wide spread acceptance worldwide for the treatment of molten steel for removal of various dissolved impurities. The RH process was originally developed for removal of hydrogen from steel. It is being utilized for decarburization, deoxidation and composition control. In addition to providing effective degassing, this process also provides an effective means of agitating the bath. The RH process is performed in a refractory lined vessel. The vessel is connected to a system of vacuum pumps capable of obtaining pressures as low as 0.5 torr. The addition of Ferro alloys during treatment is done through pressure tight weight bins and lock hoppers connected to the vessel by an alloy chute. The vessel has two refractory lined tubes (snorkels) extending from its lower part. These snorkels are used as conduit to circulate steel between the vessel and the ladle. A schematic diagram of the RH process is shown in Figure 1(a) and the dimensions used in the computation are shown in Figure 1(b).

A ladle containing non-deoxidized liquid steel is placed under the vessel. The process starts by lifting the ladle or lowering the RH vessel until the snorkels penetrate the slag layer and get immersed in the steel. In the present case the RH vessel is lowered down. The vessel is then evacuated to a low pressure. Atmospheric pressure forces steel to rise through the snorkel and occupy the lower part of the RH vessel. Argon or nitrogen lift gas is introduced into one of the snorkels (the up-leg snorkel). The motion of the lift gas causes the steel to rise in the up-leg snorkel. Thus, the steel recirculates through the vessel and returns to the ladle through the other snorkel, called the down-leg snorkel. Throughout the treatment, the ladle serves as a reservoir of the liquid steel.

During the RH process, carbon in the steel combines with dissolved oxygen to form carbon monoxide. The reaction enhances under vacuum conditions. The decarburization rate increases with a decrease in the pressure in the vessel and with the increase of reaction area and circulation rate (Hanna *et al.*, 1994; Ahrenhold and Pluschkell, 1998; Park *et al.*, 2000; Park *et al.*, 2001; Tsujino *et al.*, 1989; Inoue *et al.*, 1992). The higher the circulation rate, the higher the rate at which fresh metal is exposed to the vacuum at the surface. During the final treatment stages, deoxidizers and Ferro alloys are added to the steel in the vessel. After the steel is properly treated, the vessel returns to the atmospheric pressure, and the RH vessel is then lifted and the ladle is sent to the caster to continue the steel manufacturing process.

It has been reported in the literature (Szatkowski and Tsai, 1992) that inner diameter of the down-leg-snorkel decreases over a period of time. This is because of the slag

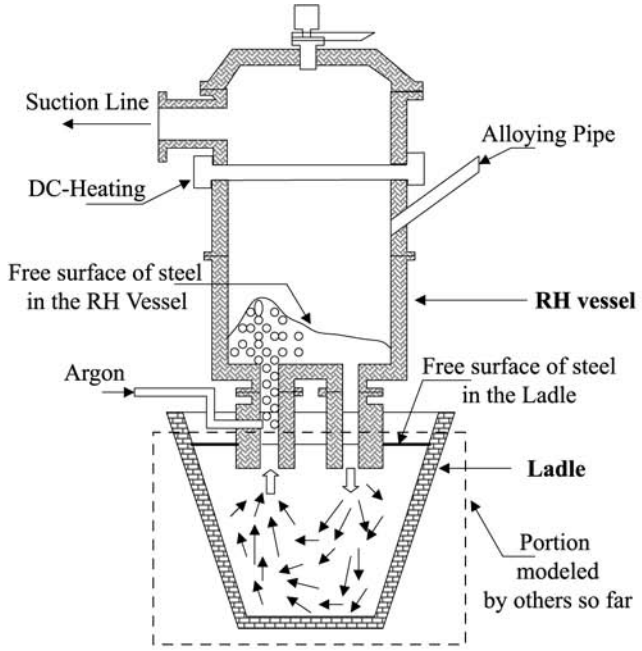

(a) Schematic diagram of a RH Degasser used in a steel making plant

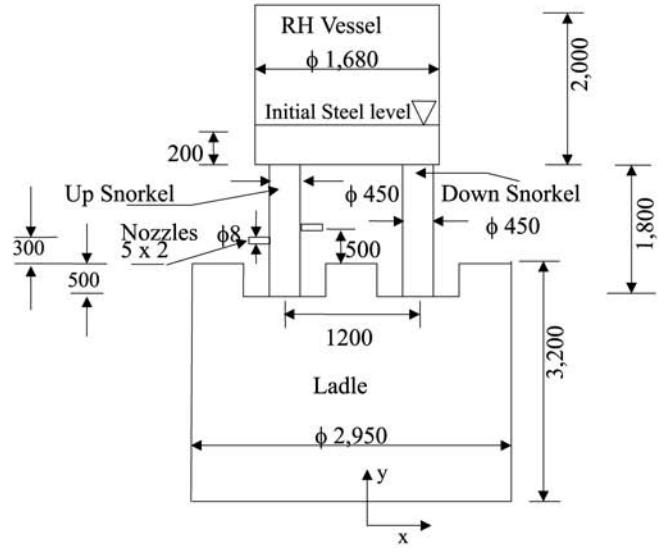

(b) Schematic diagram of RH degasser (computational domain)
All dimensions are in mm, Not to scale

Figure 1.

deposition on the inner side of the snorkel. This is known as clogging. Clogging of down-leg snorkels reduces the circulation rate. This causes improper mixing of the steel in the ladle. Efficiency of RH process depends on the circulation rate. Circulation rate influences the decarburization, deoxidation, dehydrogenation as well as mixing in the ladle. The circulation rate in the RH process depends upon the shape of the system/dimensional parameters such as snorkel diameter, radius of vacuum chamber, nozzle position and number and operating conditions such as pressure of vacuum vessel, Argon gas flow rate and the submerged depth of the snorkels (Hanna *et al.*, 1994; Ahrenhold and Pluschkell, 1998; Park *et al.*, 2001; Li and Tsukihashi, 2000).

Direct study of a real RH system to evaluate the circulation flow rate is mathematically difficult because the computational procedure needs two phase flow models which are not established very authentically even today. Therefore, in order to understand the RH system various researchers performed water model experiments (Hanna *et al.*, 1994; Li and Tsukihashi, 2000; Seshadri and De Souza Costa, 1986; Nakanishi *et al.*, 1975), mixing time measurements (Nakanishi *et al.*, 1975) in real process and numerical simulations of the ladle only (the lower part of the picture shown in Figure 1(a)), where two phase flow does not occur. (Park *et al.*, 2000; Park *et al.*, 2001; Tsujino *et al.*, 1989; Szatkowski and Tsai, 1992; Nakanishi *et al.*, 1975; Ahrenhold and Pluschkell, 1999; Shirabe and Szekely, 1983; Ajmani *et al.*, 2004). Water model experiments have been done on a 1/10-1/5 scale model in order to investigate the influence of various parameters. But the applicability of water models is limited because the operating conditions between the water model and the real systems are widely different (Hanna *et al.*, 1994; Park *et al.*, 2000; Park *et al.*, 2001). So for a realistic simulation one has to adapt to plant conditions. Circulation flow rate depends on various parameters. Empirical relations (Hanna *et al.*, 1994; Kuwabara *et al.*, 1988) do not include all these parameters. Therefore, the applicability of empirical equations is also limited. Energy balance was considered to calculate the circulation flow rate inside the RH vessel (Ahrenhold and Pluschkell, 1998; Seshadri and De Souza Costa, 1986; Kuwabara *et al.*, 1988), but the method provides always higher prediction compared to the actual system because it is difficult to account for all the energy losses in the system very accurately. Hence, Numerical studies are an alternative method to overcome experimental limitations.

In earlier works (Nakanishi *et al.*, 1975; Shirabe and Szekely, 1983), a two-dimensional numerical simulation was used to simulate fluid flow inside the ladle. Such simulations showed short-circuiting between the two legs, which is never seen in reality. To avoid this unrealism three-dimensional numerical simulations were tried (Tsujino *et al.*, 1989; Szatkowski and Tsai, 1992; Ajmani *et al.*, 2004), which could depict the flow realistically in the ladle. In the previous studies (Ahrenhold and Pluschkell, 1998; Tsujino *et al.*, 1989; Szatkowski and Tsai, 1992; Seshadri and De Souza Costa, 1986; Nakanishi *et al.*, 1975; Ajmani *et al.*, 2004), the existence of snorkels and vacuum vessel has been ignored and only the ladle portion of the RH process was considered. The governing equations were solved only for the ladle portion because two-phase flow does not occur in this region.

In the present work, an attempt has been made to simulate the entire process (ladle + RH vessel as shown in Figure 1(a) and (b)) numerically by using a two-phase flow model in a Eulerian scheme. It is to be noted that till today all the simulations on the RH have been done only for the ladle with a single phase CFD model because two-phase flow models have been really very difficult to be implemented for such

geometries due to lot of practical difficulties, one of the biggest difficulties was the computational time. In the present simulation process, argon gas will be blown through ten nozzles into the up-leg and the friction between the gas and the liquid will cause the liquid to move into the RH vessel and come down to the ladle through the down-leg thus establishing a circulation loop. The circulation flow rate thus obtained is computed as a function of the gas flow rate. To validate the numerical solution, circulation flow rate in an experimental setup (air driving water) as shown in Figure 2 has been computed and validated against the experimental observations.

Mathematical formulation

The recirculation in the bath or ladle with gas injection has been solved with a two-fluid (or two-field) Euler-Euler technique. The two-fluid method or the Eulerian-Eulerian model considers both the gas and liquid phases as continuum, with each computational cell of the domain containing respective fractions of the continuous and dispersed phases. The unsteady mass and momentum transfer of the rising bubbles to the liquid steel is considered with the following assumptions:

- The fluids in both the phases are Newtonian, viscous and incompressible.
- The physical properties are constant.
- The pressure is considered to be common to both the phases.
- The size of the gas bubbles is uniform throughout and the bubbles are introduced into the system, through a nozzle, at a given velocity.
- The interfacial surface between steel and argon in the RH vessel is not affected by surface tension.
- It is assumed that the k-ε model may be applied to describe the behavior of the mixture.

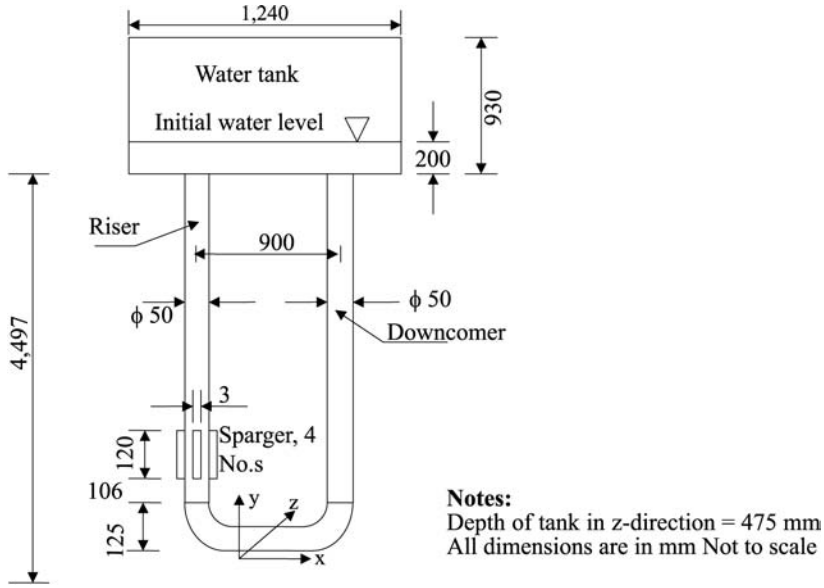

Figure 2.
Schematic diagram of the experimental setup

- Transport between the gas phase and the liquid phase may be represented in terms of an interface-friction coefficient, the numerical value of which depends on the bubble size.
- The flow is assumed to be isothermal, so the energy equations are not needed. In fact the argon, which is injected into the steel attains the same temperature like that of steel within a much shorter time compared to its average residence time in the up-leg and in the RH vessel.
- The presence of slag at the top surface of the liquid steel in the ladle is neglected in this study.

With all the above assumptions the governing equations for phase q can be written as: (Drew, 1983; Laurien *et al.*, 1999; Anglart *et al.*, 1997)

Continuity

$$\frac{\partial}{\partial t}(\alpha_q \rho_q) + \nabla \cdot (\alpha_q \rho_q \vec{v}_q) = \Gamma_q \tag{1}$$

The solution of equation (1) for each secondary phase, along with the condition that the volume fractions sum to one (as in equation (2)), allows the calculation of primary phase volume fraction:

$$\alpha_q + \alpha_p = 1 \tag{2}$$

Momentum

$$\frac{\partial}{\partial t}(\alpha_q \rho_q \vec{v}_q) + \nabla \cdot (\alpha_q \rho_q \vec{v}_q \vec{v}_p) = -\alpha_q \nabla p + \nabla \cdot (\bar{\bar{\tau}}) + \alpha_q \rho_q \vec{g} + \Gamma_q \vec{v}_{pq} + M_q \tag{3}$$

$\bar{\bar{\tau}}_q$ *is the* qth phase stress tensor:

$$\bar{\bar{\tau}}_q = \alpha_q \mu_q^{\text{eff}} \left(\nabla \vec{v}_q + \nabla v_q^T \right) \tag{4}$$

$$\mu_q^{\text{eff}} = \mu_q + \mu_{t,q} \tag{5}$$

Γ_q is the mass transfer between the phases and $\vec{v}_{pq}$is the inter-phase velocity.
The three dimensional model of unsteady, multiphase flow equations (1-3) must be supplemented with additional relationships to achieve the closure. The closure relationships used in the present model refer to two-phase bubbly flow, with continuous liquid phase and disperse gas phase.

The key issue in accurate modeling of multiphase flows is to specify interaction terms (Γ_q, M_q). If incompressible material with no phase change is considered then, $\Gamma_q = 0$ and ρ_q = constant.

Interfacial effects
As already mentioned, the phase interaction term, which are source terms in equations (1) and (3) are the interfacial mass transfer term Γ_q, interfacial momentum transfer term, M_q.

Specifically:

$$M_q = M_q^{\text{d}} + M_q^{\text{VM}} + M_q^{\text{L}} \tag{6}$$

where the individual terms on the right hand side of equation (6) are, the drag force, virtual mass force, and the lift force, respectively.

The first term represents drag force, which results from unequal velocities between the two phases. Drag between a fast moving bubble and slow moving liquid, for instance, tends to slow down the bubble and speed up the surrounding liquid as well as cause some frictional heating of both phases due to viscous dissipation. The interfacial drag force is given by (*FLUENT 6.1 Manual*, 2003):

$$M^{\mathrm{d}} = \frac{3}{4} C_{\mathrm{D}} Re \frac{(\alpha_p \mu_p + \alpha_q \mu_q)}{\left(\frac{d_p + d_q}{2}\right)^2} (\vec{v}_p - \vec{v}_q) \tag{7}$$

Relative Reynolds number for primary phase q and secondary phase p is given by:

$$Re = \frac{\rho_q |\vec{v}_q - \vec{v}_p| d_p}{\mu_q} \tag{8}$$

The velocity difference between the phases is broken up using the absolute value sign as shown in Re to ensure that the drag force is positive on the slower moving phase, and negative on the faster moving phase. It is assumed that the droplets or bubbles are small enough to be nearly spherical. The drag coefficient C_{D} depends on the particle Reynolds number and can be written as (Wallis, 1969; Gidaspow, 1994):

$$\begin{aligned} C_{\mathrm{D}} &= 24(1 + 0.15Re^{0.687})/Re \quad Re \leq 1,000 \\ &= 0.44 \qquad\qquad\qquad\quad Re > 1,000 \end{aligned} \tag{9}$$

The second term in equation (6) represents the virtual mass force. When a gas bubble accelerates through the liquid, it experiences a resistance force due to the liquid it displaces. This induces an apparent increase in bubble inertia.

The virtual mass force is given by (Anglart *et al.*, 1997; Milelli, 2002):

$$M_q^{\mathrm{VM}} = -M_p^{\mathrm{VM}} = C_{\mathrm{VM}} \alpha_p \rho_q \left(\frac{d_q \vec{v}_q}{\mathrm{d}t} - \frac{d_p \vec{v}_p}{\mathrm{d}t} \right) \tag{10}$$

The term $d_q/\mathrm{d}t$ denotes the phase material time derivative. The virtual mass effect is significant when the secondary phase density is much smaller than the primary phase density. The virtual mass coefficient, C_{VM}, for potential flow around a sphere is 0.5. In reality bubbles will usually not be spherical, but of more oblate shape. The third term in equation (6) is the lift force, which arises from a velocity gradient of the continuous phase in the lateral direction.

If a particle (bubble) with a rigid surface moves in a non-uniform flow field, the asymmetry of the wake causes an additional force of interaction, perpendicular to the main flow direction. This force is proportional to the relative velocity and to the liquid vorticity. Lift force can be written according to the references Laurien *et al.* (1999), Anglart *et al.* (1997) and Smith (1998) as:

$$M_q^{\mathrm{L}} = -M_p^{\mathrm{L}} = C_{\mathrm{L}} \rho_q \alpha_p (\vec{v}_p - \vec{v}_q) \times (\nabla \times \vec{v}_q) \tag{11}$$

For spherical bubbles, lift coefficient $C_{\mathrm{L}} = 0.5$. The coefficient can vary from 0.4 to 0.6.

Turbulence modeling

Turbulence modeling for two-phase flow requires considerable further development. There is no industrial standard model such as the k-ε model for single-phase flow. The turbulence in the liquid phase has a strong influence on the void fraction distribution, and phenomena such as bubble flattening, break-up and wobble and all these phenomena will have effects on the turbulent kinetic energy production.

Constant eddy-viscosity models are used successful in bubble-plume applications. The current trend is to solve transport equations for the turbulence quantities, with the k-ε model for two-phase also. Owing to the lack of additional information for two phase flows, and because the model must reduce to k-ε model for the single phase flows, the constants $C_{1\varepsilon}$, $C_{2\varepsilon}$, σ_ε are same as in the standard k-ε model for single phase flows. k-ε model with standard (single phase) coefficients can be used when the two-fluid model is adopted for flow calculations.

Turbulent kinetic energy – k (FLUENT 6.1 Manual, 2003)

$$\frac{\partial}{\partial t}(\rho_{\mathrm{m}}k) + \nabla\cdot(\rho_{\mathrm{m}}\vec{v}_{\mathrm{m}}k) = \nabla\cdot\left(\frac{\mu_{\mathrm{t,m}}}{\sigma_k}\nabla k\right) + G_{k,\mathrm{m}} - \rho_{\mathrm{m}}\varepsilon \tag{12}$$

Rate of dissipation of k

$$\frac{\partial}{\partial t}(\rho_{\mathrm{m}}\varepsilon) + \nabla\cdot(\rho_{\mathrm{m}}\vec{v}_{\mathrm{m}}\varepsilon) = \nabla\cdot\left(\frac{\mu_{\mathrm{t,m}}}{\sigma_\varepsilon}\nabla\varepsilon\right) + \frac{\varepsilon}{k}(C_{1\varepsilon}G_{k,\mathrm{m}} - C_{2\varepsilon}\rho_{\mathrm{m}}\varepsilon) \tag{13}$$

Where the mixture density and velocity ρ_{m} and $\vec{v}_{\mathrm{m}}$, are computed from:

$$\rho_{\mathrm{m}} = \alpha_p\rho_p + \alpha_q\rho_q \tag{14}$$

$$\vec{v}_{\mathrm{m}} = \frac{\alpha_p\rho_p\vec{v}_p + \alpha_q\rho_q\vec{v}_q}{\alpha_p\rho_p + \alpha_q\rho_q} \tag{15}$$

The turbulent viscosity $\mu_{\mathrm{t,m}}$ is computed from:

$$\mu_{\mathrm{t,m}} = \rho_{\mathrm{m}}C_\mu\frac{k^2}{\varepsilon} \tag{16}$$

and the production of turbulent kinetic energy, $G_{k,m}$ is computed from:

$$G_{k,\mathrm{m}} = \mu_{\mathrm{t,m}}\left(\nabla\vec{v}_{\mathrm{m}} + \left(\nabla\vec{v}_{\mathrm{m}}\right)^T\right) : \nabla\vec{v}_{\mathrm{m}} \tag{17}$$

The constants in the above equations are $C_{1\varepsilon} = 1.44$; $C_{2\varepsilon} = 1.92$; $C_\mu = 0.09$; $\sigma_k = 1.0$; $\sigma_\varepsilon = 1.3$

Boundary conditions

At the ladle, snorkels and vacuum vessel walls, no slip condition was considered and wall functions were employed for the turbulent quantities.

At the entrance of the nozzles, velocity of argon was given as input with mass fraction of liquid steel to be zero.

At the top of vacuum vessel, zero pressure was considered which means that the argon gas is leaving the domain at an external relative pressure of 0.0.

The free surface of molten steel in the ladle was exposed to the ambient where a wall boundary condition was applied. In practice the slag layer sitting over there creates a wall effect so in the mathematical model it is justified to take a wall condition. Even the symmetry condition can be taken also without much of an error being introduced into the computation.

Numerical solution procedure

The three-dimensional equations of mass, momentum, volume fraction and turbulent quantities along with the boundary conditions have been integrated over a control volume and the subsequent equations have been discretized over the control volume using a finite volume technique to yield algebraic equations which can be solved in an iterative manner for each time step. The discretization form for all the convective variables was taken to be first order up winding initially for better convergence. Slowly as time progressed the discretization forms were switched over to second order up winding and then slowly towards the QUICK scheme for better accuracy. It is to be noted that the virtual mass force and the lift force are not be switched on from the beginning of computation because they could initiate instability. Once the computation proceeds for a long time such forces could be switched on and the solution accuracy will not be spoiled due to this because we are looking for a steady state solution in any case. Transient solution probably does not have much physical meaning in such practical problems unless some one is academically interested to find some particular phenomenon during the solution process. The Phase Coupled SIMPLE (an extension of SIMPLE) algorithm for the pressure-velocity coupling was used for the pressure correction equations. The velocities were solved coupled by the phases, but in a segregated fashion. The block algebraic multi grid scheme of Fluent was used to solve all the algebraic equations. The pressure correction equation was built based on total volume continuity rather than on mass continuity. Pressure and velocities were then corrected so as to satisfy the continuity constraint.

Fine grids were used where both the phases were present. A grid arrangement at the initial stage of the solution is shown in Figure 3 (a) and (b) and later on when the

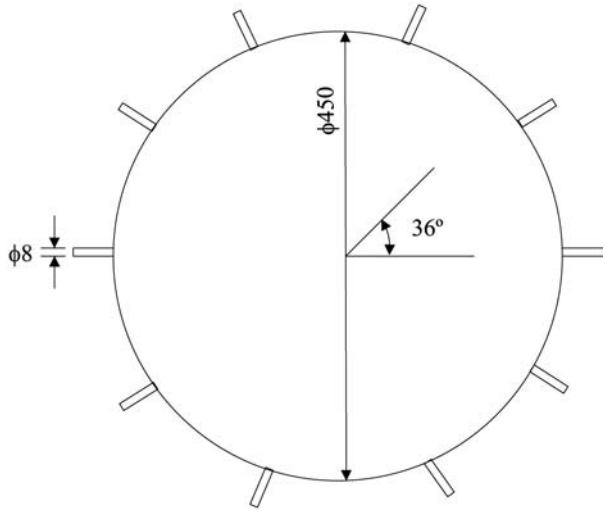

Figure 3.
Plan view of nozzles arrangement in the upleg

solution progressed with time the grids were refined near the interfaces to obtain better accuracy. Near the nozzle inlet the grids were tetrahedral and away from the nozzles hexahedral grids could be placed to have better accuracy. Owing to the connection problems of the nozzles with the up-leg tetrahedral cells were placed near the nozzles although this type of cells reduce the accuracy of the solution to some extent. The nozzle arrangement near the up-leg can be seen in Figure 4 where two rows of nozzles (five in each row) are shown on a plan view. The first row of nozzles is 300 mm away from the top surface of the ladle and the second row of nozzles are 500 mm away. However, most of the domain contains hexahedral cells and they were slowly refined with time to capture the volume fraction of the gas and turbulence little more accurately. The time step used in the solution was about 1×10^{-5} s initially and after a time of 0.2 s the time step was changed to 2×10^{-5} and then after 0.6 s to 4×10^{-5} s to reduce the total computational time. With this kind of time step the entire computation with one gas flow rate took about a month to be completed (on a Pentium IV 3.2 GHz machine with 2 GB RAM). A complete solution for one gas flow rate means when the solution could attain a steady state so that the circulation flow rate within the system did not change by 0.1 percent. To start with there were about 64,000 cells in the RH computation and that slowly grew to about 160,000 when the computation could proceed with time. The same number of cells was almost present in the computation done for the experimental setup also. The physical properties of the fluids those were used in the computation could be read from Table I.

Results and discussions

The numerical model before being applied to the RH degasser for circulation flow rate due to argon injection was first tested for an experimental setup where air was injected into the U tube through the sparger and water could be lifted up due to this. The entire experimental setup with the details of the dimensions used in the computation is shown in Figure 2. The initial water level in the tank was maintained at 200 mm from the bottom of the tank and the airflow into the sparger was varied from 0.3 to 2.0 Lt/s (at 25°C, 1 atm). The riser and the down comer tubes were connected symmetrically at the mid section and to the bottom of the upper tank which, is not shown in the drawing.

Experimental validation

Figure 5 shows the volume fraction of air in the experimental setup when steady state was achieved. It can be seen from the figure that there is air at the upper portion of the tank (red color indicates pure air with volume fraction = 1) and the interface is undulated where the air jet from the riser is hitting it. When the air jet comes out of the water it pulls some amount of water with it so the free surface of water becomes undulated or looks like "hat" shaped. The same kind of shape could be seen in the experiment but due to the absence of surface tension forces in the numerical model the hat shaped region looks little more triangular which is little unrealistic. Figure 6 shows the expanded view of the U tube and the sparger and the flow of air through it. It can be seen that, at the sparger the air volume fraction is high (which is indicated by red color) and slowly it reduces along the walls of the U tube and thereafter remains constant. The air rises along the wall of the tube and at the center of the tube water flows through. Figure 7 shows the velocity vector in the riser and also in the down comer for an airflow rate of 1.2 NL/s. It can be marked from the figure that there is a steady circulation flow of

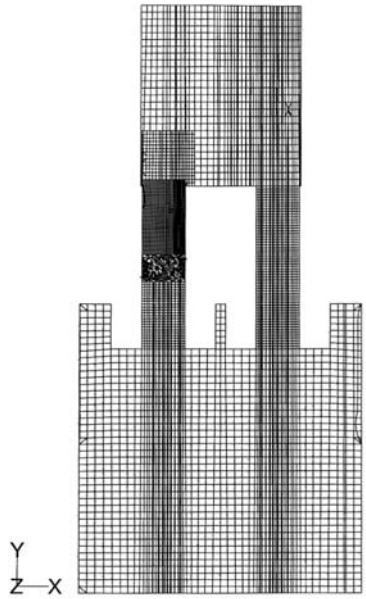

(a) Grid arrangement in a vertical cross sectional plane (z = 0) through the RH

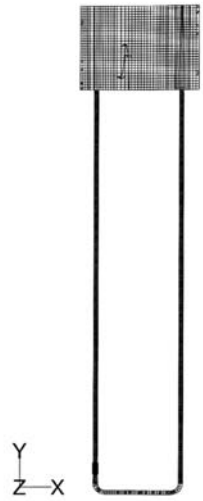

(b) Grid arrangement in a vertical cross sectional plane (z = 0) through the experimental setup

Figure 4.

Table I.
Properties of the fluids used in the computation

Property	Water	Steel	Air	Argon
μ (kg-m/s)	0.001	0.00642	1.789×10^{-5}	2.125×10^{-5}
ρ (kg/m^3)	998.2	7,100	1.225	1.622

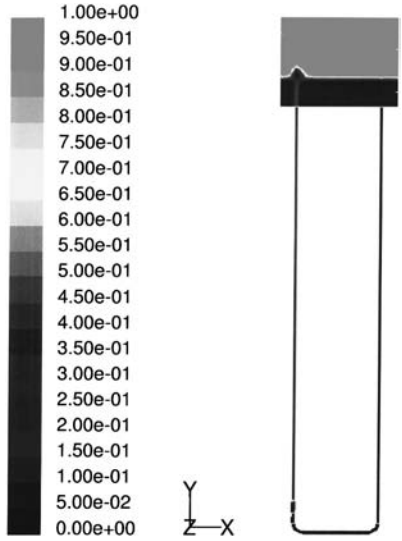

Figure 5.
Contours of volume fractions of air in the experimental setup at $z = 0$ vertical cross-sectional plane ($\dot{Q}_{air} = 1.2$ NL/s)

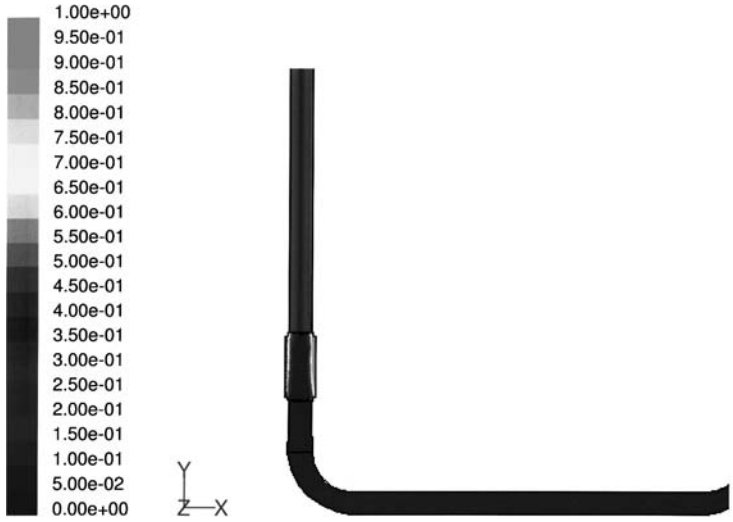

Figure 6.
Contours of volume fractions of air near the sparger, $\dot{Q}_{air} = 1.2$ NL/s

water in the U tube where it comes down through the down comer and rises up to the tank again through the riser. Figure 8 shows the volume fraction of water and air in the tank along with the velocity distribution in the tank at the vertical cross sectional plane of $z = 0$. In the tank the bottom portion is occupied by water and that is shown in red color while the top portion is occupied by air and that is shown by blue color. The interface is seen to be very sharp where the color changes from red to blue very sharply through yellow and green representing a sharp gradient of water to air. Near the air jet at the riser tube there is an entrainment zone where the fluid is entrained into the air jet and

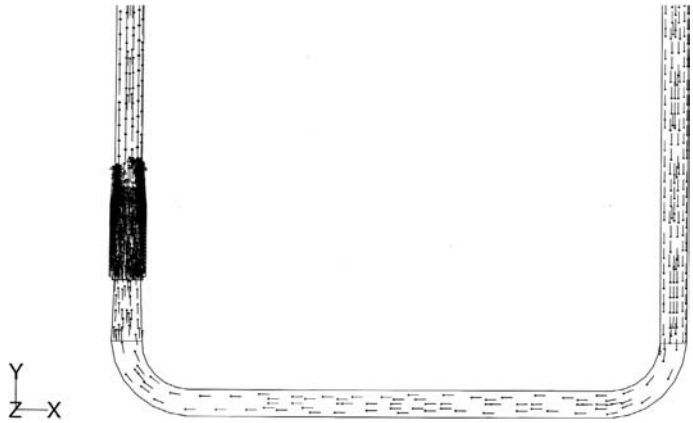

Figure 7.
Computed flow pattern in the riser and down-comer for the experimental setup, ($\dot{Q}_{air} = 1.2$ NL/s)

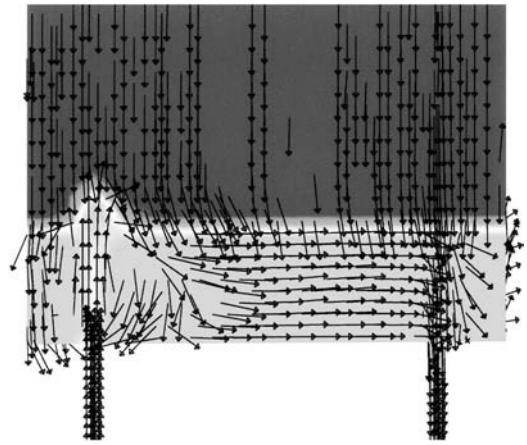

Figure 8.
Velocity field at the free surface of water in the experimental setup at $z = 0$ plane, ($\dot{Q}_{air} = 1.2$ NL/s)

this is the main reason for circulation flow to persist. The air diffuses at the free surface and fresh air is being sucked in from the atmosphere through the upper free surface. Water, which is entrained at the air jet, forms a circulation loop in the tank and passes through the down comer and finally to the riser again.

Figure 9 shows the comparison of circulation flow rate of water between the experiment and that of the computation when the airflow rate was varied from 0.3 to 2.0 NL/s. From the figure, it can be concluded that the mathematical model very nearly catches up to the experimental measurement although there is ample scope for the mathematical model to improve upon. The circulation flow rate within the system can also be computed from simple energy balance, which can be found in detail in reference (Rao, 2002). In this method the pressure drop at the sparger entry, pressure drop at the walls of the riser and down comer, expansion loss at the entry into the tank and contraction loss at the down comer is taken into account to arrive at the circulation of water in the tube. Such a computation is also shown in Figure 9 along with the present CFD computation and the experimental result. It can be seen from the figure that the

energy balance method predicts always higher circulation flow rate. This is due to the fact that accurate accounting of all the pressure drops in the system is not possible mathematically and the energy loss at the free surface has not been modeled in reference (Rao, 2002). In fact reference Rao (2002) has to depend on empirical correlations for pressure drop so as to develop an energy balance method for the experimental setup. However, the energy balance method in the absence of experiment or CFD computation can provide a guideline to the maximum circulation flow rate that can be achieved in a particular system.

Circulation flow in the RH ladle and vessel

Figure 10 shows the contours of volume fraction of argon in the entire RH ladle as well as the RH vessel at a vertical cross sectional plane of the vessel ($z = 0$) due to the blowing of argon (red color contour) from the ten nozzles, which are placed in two rows on the up-leg with five nozzles in each row. It can be seen from the figure that the argon gas immediately rises up along the wall through the up-leg straight up to the free surface and hence drags the liquid steel along with it. There is a recirculation of liquid steel in the up-leg itself, which can be seen from Figure 11 in an expanded view. On the free surface there is not much oscillation found but a small wave of the liquid is present. In the case of the RH, the up-leg is 450 mm in diameter compared to the case of the experimental setup where it was just 50 mm. So the air that was coming through the up-leg up to the free surface was coming like a jet and hence was creating a big surface wave on the free surface. But in the RH the amount of argon that is passing through the up-leg is getting a chance to spread all over the cross sectional area of the up-leg and hence does not come up like a jet to the free surface so there is not much of surface wave on the free surface. From Figure 11, it can be seen that between the up-leg and the down-leg there is a recirculating loop of liquid steel and through the down-leg there is a steady flow towards the ladle. The red color in Figure 11 shows the liquid steel and the blue color the argon gas.

Figure 12 shows the velocity field in the ladle through the vertical cross sectional plane at $z = 0$. It can be seen that there are two distinct streams of flow in the ladle. One is the up-leg flow and the other the down-leg flow. Inside the RH ladle, there is flow everywhere but the magnitude of the velocity elsewhere is much lower compared to the zones, which are directly under the up-leg and the down-leg.

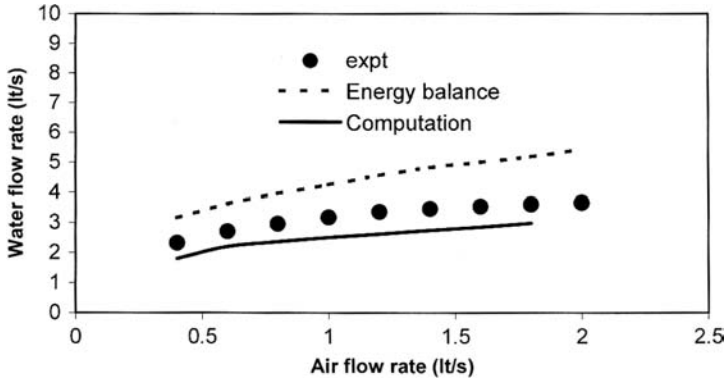

Figure 9.
A comparison between computed and experimentally measured circulation flow rate of water as a function of air flow rate

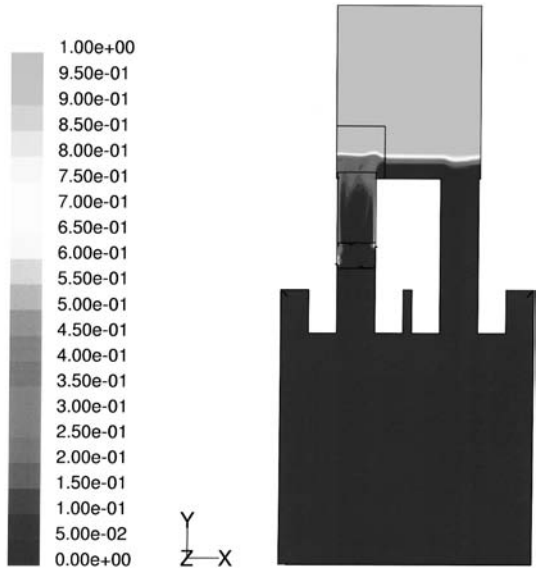

Figure 10.
Contours of volume fraction of argon in the RH degasser at $z = 0$ plane, ($\dot{Q}_{ar} = 1{,}600$ NL/min)

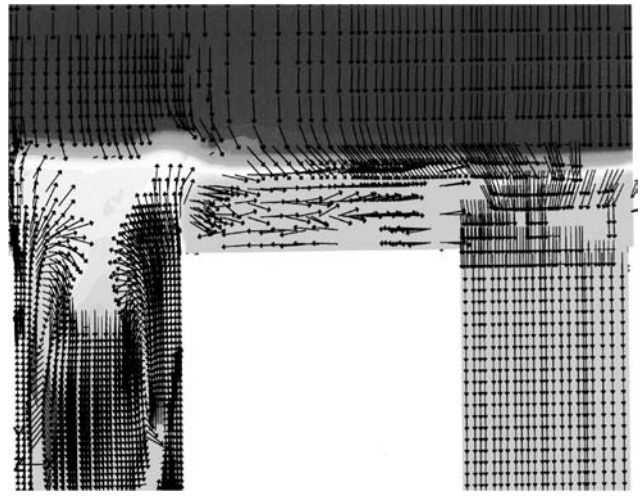

Figure 11.
Velocity field at the free surface of molten steel in the RH vessel at $z = 0$ plane, ($\dot{Q}_{ar} = 1{,}600$ NL/min)

Figure 13 shows the graph of circulation flow of liquid steel in the RH vessel as a function of argon gas flow rate. It can be seen from the figure that the circulation flow rate does not increase much if the argon flow rate increases beyond 1,400 NL/min. When the gas flow is high in the up-leg there is a stronger recirculation also in the up-leg which hindrances the flow of liquid to take place smoothly into the RH vessel from the ladle for which the circulation flow rate attains a limiting value. If the arrangement of the nozzles are changed or the diameter of the up-leg is changed it is expected that the flow of steel will increase in the ladle, which is normally found in the plant practices. The energy balance equations also predict the circulation flow rate

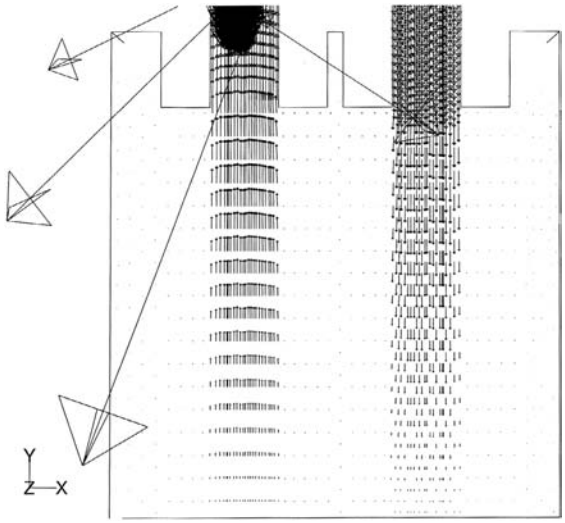

Figure 12.
Velocity field of molten steel inside the ladle at $z = 0$ plane, ($\dot{Q}_{ar} = 1{,}600$ NL/min)

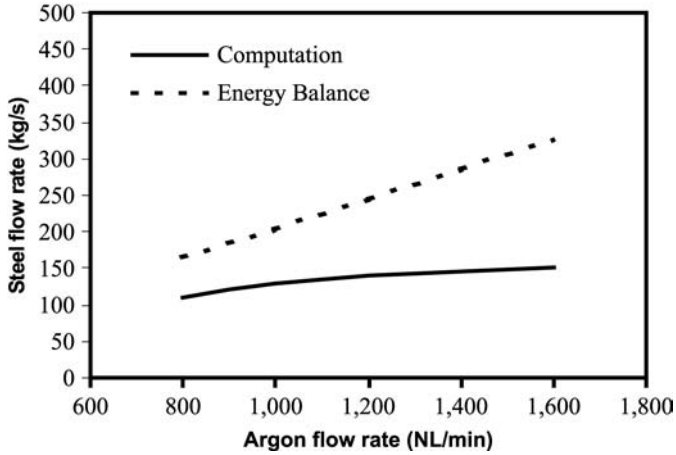

Figure 13.
Variation of circulation flow rate of steel as a function of argon flow rate in the RH degasser

here, which is shown in the same Figure 13. But it can be seen that like the previous findings the energy balance equations predict much higher circulation flow rate in the RH system. The equations those are utilized to generate the flow rate in the ladle from the energy balance considerations are shown in the Appendix. The energy losses that is taking place at the free surface is much higher compared to the losses that is taking place due to wall friction, expansion at the up-leg and contraction at the down comer. The energy loss at the free surface increases tremendously as the gas flow rate increases. So if the losses at the free surface are not taken into account then the deviation between the CFD result and the energy balance method will be much larger, which has been shown in Figure 13. In the absence of a model, to account for accurate representation of energy losses at the free surface, one cannot predict accurately the

circulation flow rate in the vessel. However, the energy equations always can be used to predict a limiting higher value of circulation flow rate in the system in the absence of any other CFD models or experiments.

Difficulty to reproduce plant result

In the actual plant practice the circulation flow rate in the RH vessel is much higher compared to what has been shown in Figure 13. In the present CFD model the expansion of the argon gas due to sudden heating in the liquid steel is not taken into account due to several difficulties. Had that been taken into account then the circulation flow rate would have been much higher. In order to take the expansion of the gas in the liquid steel one has to solve the energy equation and that adds to computer time, which was found almost impossible with our computers. The gas within a very short time attains the temperature of liquid steel (about 1,773 K) inside the bath and hence expands to about 15 times inside the liquid bath. So in order to take into account this effect one has to use a very fine grid at the nozzle inlet and use extremely small time step, which considerably increases the computational time and also the computation becomes unstable for even 800 Lt/min of argon flow which is the bare minimum flow for an industrial setup. So it was almost impossible to get a feasible solution with the energy equation being activated along with all other equations in place. Otherwise also one could try to put higher nozzle inlet velocity for argon to take into account higher volume flow of argon inside the bath. This process also calls for instability because the inlet velocities become as large as 250 to 300 m/s at the inlet of each nozzle for the minimum argon flow of 800 Lt/min in a real plant case. So a practical solution of the plant case with or without the energy equation being solved looks very difficult for the time being. However, the present method is a step towards that which can predict at least the circulation flow rate in a RH vessel from first principles with the use of CFD with very little empiricism in the CFD model (only empirical formula being used is the drag law).

Conclusions

The conservation of mass and momentum equations (with suitable source terms to represent interfacial drag, lift and virtual mass forces) have been solved numerically with the k-ε model; using an unstructured grid; to predict the flow field and the distribution of the liquid and gas phase volume fraction inside the experimental set up as well as for the RH ladle and vessel. By using the flow field the circulation flow inside the devices could be computed for various gas flow rates. It could be concluded from the present study that the two-phase numerical model is able to predict the circulation flow rate to within 15 percent accuracy compared to the experimental observation. However, it has not been possible to perform an exact numerical simulation for the plant case taking into account the expansion of argon gas inside the RH due to several practical difficulties. But the present computation is a realistic step towards the exact computation of the plant case because the present simulation is a computation from the first principle without much empiricism imbedded in it.

References

Ahrenhold, F. and Pluschkell, W. (1998), "Circulation rate of liquid steel in RH degassers", *Steel Research*, Vol. 69, pp. 54-9.

Ahrenhold, F. and Pluschkell, W. (1999), "Mixing phenomena inside the ladle during RH decarburization of steel melts", *Steel Research*, Vol. 70, pp. 314-8.

Ajmani, S.K., Dash, S.K., Chandra, S. and Bhanu, C. (2004), "Mixing evalution in RH process using mathematical modelling", *ISIJ International*, Vol. 44, pp. 82-90.

Anglart, H., Nylund, O., Kurul, N. and Podowski, M.Z. (1997), "CFD prediction of flow and phase distribution in fuel assemblies with spacers", *Nuclear Engineering and Design*, Vol. 177, pp. 215-28.

Drew, D.A. (1983), "Mathematical modeling of two-phase flows", *Ann. Rev. Fluid Mech.*, Vol. 15, pp. 261-91.

FLUENT 6.1 Manual (2003), Lebanon, NH.

Gidaspow, D. (1994), *Multiphase Flow and Fluidization: Continuum and Kinetic Theory Descriptions*, Academic Press, Boston, MA.

Hanna, R.K., Jones, T., Blake, R.I. and Milliman, M.S. (1994), "Water modelling to aid improvement of degasser performance for production of ultralow carbon interstitial free steels", *Ironmaking and Steelmaking*, Vol. 21, pp. 37-43.

Inoue, S., Furuno, Y., Usui, T. and Miyahara, S. (1992), "Acceleration of decarburization in RH vacuum degassing process", *ISIJ International*, Vol. 32, pp. 120-5.

Kuwabara, T., Umezawa, K., Mori, K. and Watanabe, H. (1988), "Investigation of decarburisation behaviour in RH – reactor operation improvement", *ISIJ International*, Vol. 28, pp. 305-14.

Laurien, E., Becker, S., Saptodi, D. and Giese, T. (1999), "Multidimensional modelling of bubbly flows for nuclear reactor passive decay heat removal", paper presented at Eurotherm Seminar No. 63: Single and Two-phase Natural Circulation, 6-8, September, Genua (in Italien).

Li, B. and Tsukihashi, F. (2000), "Modeling of circulating flow in RH degassing vessel water model designed for two- and multi-legs operations", *ISIJ International*, Vol. 40, pp. 1203-9.

Milelli, M. (2002) Doctor of Technical Sciences thesis, Swiss Federal Institute Of Technology, Zurich.

Nakanishi, K., Szekely, J. and Chang, C.W. (1975), "Experimental and theoretical investigation of mixing phenomena in RH-vacuum process", *Ironmaking and Steelmaking*, No. 2, Quarterly, pp. 115-24.

Park, Y., Doo, W., Yi, K. and An, S. (2000), "Numerical calculation of circulation flow rate in degassing Reinstahl-Heraeus process", *ISIJ International*, Vol. 40, pp. 749-55.

Park, Y., Woo, K. and Ahn, S. (2001), "The effect of operating parameters and dimensions of the RH system on melt circulation using numerical calculations", *ISIJ International*, Vol. 41, pp. 403-9.

Rao, N.M. (2002), "Investigations on buoyancy induced circulation loops", PhD thesis, IIT, Kharagpur.

Seshadri, V. and De Souza Costa, S. (1986), "Cold model studies of RH degassing process", *ISIJ International*, Vol. 26, pp. 133-8.

Shirabe, K. and Szekely, J. (1983), "A mathematical model of fluid flow and inclusion coalescence in RH vacuum degassing system", *ISIJ International*, Vol. 23, pp. 465-74.

Smith, B.L. (1998), "On the modeling of bubble plumes in a liquid pool", *Applied Mathematical Modeling*, Vol. 22, pp. 773-97.

Szatkowski, M. and Tsai, M.C. (1992), "Turbulent flow and mixing phenomena in RH ladles: effects of clogged downleg snorkel", *ISS Transactions*, Vol. 13, pp. 33-9.

Tsujino, R., Nakashima, J., Hirai, M. and Sawada, I. (1989), "Numerical analysis of molten steel flow in ladle of RH Process", *ISIJ International*, Vol. 29, pp. 585-9.

Wallis, G.B. (1969), *One Dimensional Two-phase Flow*, McGraw Hill, NewYork, NY.

Appendix. Application of energy balance to the calculation of circulation flow rate (Seshadri and De Souza Costa, 1986)

The circulation flow rate can also be calculated by making an energy balance in the model, considering that the energy of the injected gas is utilized for the energy loss in the system by friction or expansion and contraction as well as for increasing the kinetic energy of liquid. Locations where energy loss can take place are shown in a schematic diagram (Figure A1).

If the total energy carried by the gas in the up-leg is W then, $\mathrm{d}W$ can be written in terms of pressure as:

$$\mathrm{d}W = V\mathrm{d}P \tag{A1}$$

$$-W = NRT \cdot \ln \frac{P_2}{P_1} \tag{A2}$$

$$N = \frac{Q}{22.4} \times \frac{1}{60} = \frac{Q}{1,344} \tag{A3}$$

$$W = \frac{-Q}{1,344} RT \cdot \ln \frac{P_2}{P_1} \tag{A4}$$

Where N is number of moles of gas, R is gas constant, T is temperature, P_1 is pressure at the inlet nozzle and P_2 is the pressure at the vacuum chamber.

Energy utilized in the circulation of liquid is given by equations (A5-A8)

Friction energy loss is given as:

$$F_{\mathrm{fr}} = \frac{\pi}{8} \rho D_{\mathrm{d}}^2 V^3 \cdot 4\mathrm{fr} \left(\frac{L}{D_{\mathrm{d}}} + \frac{L}{D_{\mathrm{u}}} \frac{D_{\mathrm{d}}^4}{D_{\mathrm{u}}^4} \right) \tag{A5}$$

Expansion energy loss is given as:

$$F_{\mathrm{ex}} = \frac{\pi}{8} \rho D_{\mathrm{d}}^2 V^3 \xi \left(1 + \frac{D_{\mathrm{d}}^4}{D_{\mathrm{u}}^4} \right) \tag{A6}$$

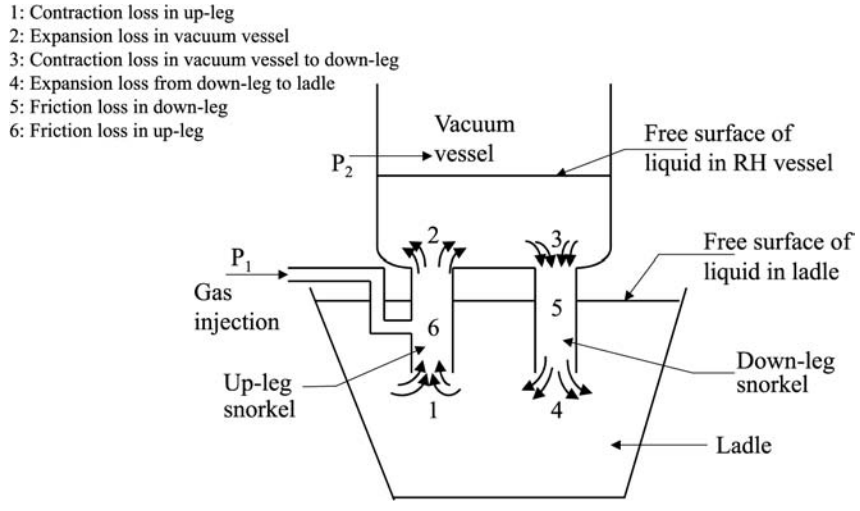

Figure A1.
Energy losses in RH degassing process

Contraction energy loss is given as:

$$F_c = F_{ex} = \frac{\pi}{8}\rho D_d^2 V^3 \eta\left(1 + \frac{D_d^4}{D_u^4}\right) \quad \text{(A7)}$$

Kinetic energy of the liquid is given as:

$$F_k = F_{ex} = \frac{\pi}{8}\rho D_d^2 V^3 \quad \text{(A8)}$$

$$W = F_{fr} + F_{ex} + F_c + F_k \quad \text{(A9)}$$

Equation (A9) is valid if there is no other energy loss at the free surface including splashing. Here, in this appendix the energy loss due to "splash" is not taken into account because that is simply not known. The splash energy loss increases with the increase of gas injection rate. By using equation (A9) one can find the liquid steel velocity, V, approximately in a system where circulation flow occurs (Table AI).

Symbol	Unit	Numerical value
Q: gas injection rate	NL/min	800-1,600
T: absolute temperature	K	293
D_d: down leg diameter	m	0.45
D_u: up-leg diameter	m	0.45
η: contraction coefficient	Dimensionless	0.45
ξ: expansion coefficient	Dimensionless	1.0
L: length of legs	m	1.8
fr: friction factor	m	0.006
ρ: density of molten steel	Kg/m^3	7,100

Table AI.
Physical dimensions and properties used for energy balance

Corresponding author
Sukanta K Dash can be contacted at: sdash@mech.iitkgp.ernet.in